Supporting Online Material

1 Sock formation

In case of spinning with a larger diameter reactor tube, a cloud with a distinct bright circumferential ring can be observed in the hot zone, with an empty space between this ring and the reactor tube wall. This cloud is supposedly either composed of only Fe particles or Fe particles which are just at the state of CNT nucleation, but probably before the formation of long CNTs. We attribute this bright circumference to a highly concentrated ring of big catalyst particles, which is ultimately responsible for the cluster impurity formation under standard conditions, similar to the annular ring described by [1]. This ring can be observed to increase with higher H_2 flow. However, in the narrow reactor tube, no such ring could be observed, but rather a cloud filling the whole cross section of the reactor tube. Even by reducing the H_2 flow to 0.3 l/min no annular ring could be observed. Hence, this cloud contains smaller, quite evenly distributed particles which don't grow big enough to form a concentrated annular ring. If there are bigger diameter particles present in the cloud, they are mixed with the smaller diameters rather than concentrated in a ring. Hence, when impurities were observed, as were when the H_2 flow was decreased significantly, these impurities were individual badly formed, almost curly structure but not clustered together (Figure 6c).

2 Conversion rates

The carbon input from the precursors is shown in Table 1 for the three samples presented. Assuming the sulphur amount in the fibre to be negligible, the amount of Fe and C can be calculated as

$$m_{Carbon} = v \cdot \rho_l \, (100\% - m_{f,Fe})$$

$$\text{with} \quad m_{f,Fe} = 69.943\% \, m_{f,Fe2O3}$$

with the winding speed v, the linear density ρ_l which was measured vibroscopically in the Favimat tensile tester, and the residue $m_{f,Fe2O3}$ known from TGA.

Table 1: Carbon input from precursors and output in form of CNT fibre

		Sample 1, impure (standard conditions)	Sample 2 (Standard chemistry, steeper velocity profile sample)	Sample 3 (Early carbon (toluene), low sulphur sample)
"Carbon in" (from Ferrocene, Thiophene, Hydrocarbon)	**[mol/min]**	**0.0034**	**0.0034**	**0.0002**
winding speed v	[m/min]	30	30	20
linear density ρ_l	[tex = g/km]	0.025	0.026	0.038
Fe_2O_3 residue from TGA		15.80%	1.50%	3%
Fe = 69.94% Fe_2O_3		11.051%	1.05%	2.10%
"Carbon out" (S or other elements not considered)	[mg/min]	0.67	0.77	0.74
	[mol/min]	**5.6E-05**	**6.4E-05**	**6.2E-05**
C-Conversion efficiency		**1.6%**	**1.9%**	**36.4%**

For a ferrocene injection rate of 0.34 mg/min (0.10 mg/min Fe), we find that for standard conditions > 80% of the iron can be accounted for in the fibre. For higher volumetric flow through the furnace, the iron included into the fibre is reduced by factor of 10.

Table 2: Iron input from ferrocene and iron amount in CNT fibre

		Sample 1, impure (standard conditions)	Sample 2 (Standard chemistry, steeper velocity profile sample)	Sample 3 (Early carbon (toluene), low sulphur sample)
Ferrocene in	[mg/min]	0.34	0.34	1.02
"Iron in" from Ferrocene $C_{10}H_{10}Fe$	[mg/min]	0.101	0.101	0.307
	[mol/min]	**1.8E-06**	**1.8E-06**	**5.5E-06**
"Iron out" (Fe = 69.94% Fe_2O_3 in TGA)	[mg/min]	0.080	0.008	0.016
	[mol/min]	**1.4E-06**	**1.5E-07**	**2.9E-07**
Fe in product		**81.9%**	**8.1%**	**5.2%**
V_f of Fe in CNT fibre ('mols $_{Fe\ out}$' / 'mols $_{Carbon\ out}$')		2.5%	0.2%	0.5%

3 Identification of TGA peaks

Thermogravimatric analysis for uncondensed standard material was measured in air with a ramp 20°C/min up to 500°C, 5°C/min from 500 to 800°C, 20°C/min up to 1000°C. The TGA analysis of impure CNT films in Figure 5 shows two very distinct peaks at 559°C and at 679°C, burning 37% and 38% of the material, respectively. It was shown in SEM by inspecting the films before (Figure S1a,b) and after TGA up to 600°C (Figure S1c,d), that the two burning events can be attributed to the impurities or the clean CNT bundles burning, respectively.

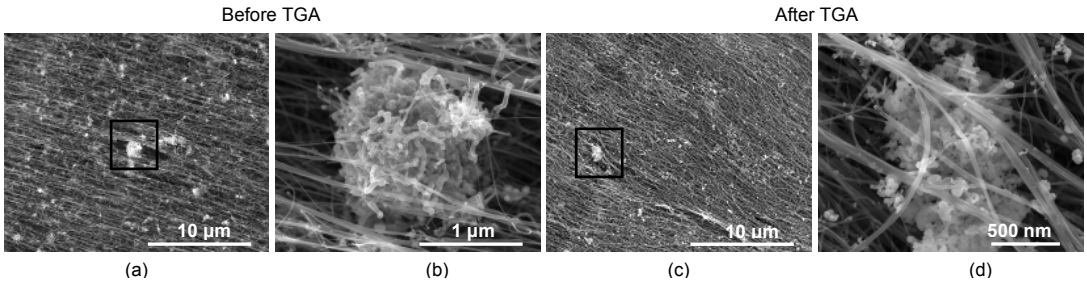

Figure S1: SEM pictures of uncondensed CNT film before (a,b) TGA and after (c,d) TGA in air up to 600 ℃. Clearly the CNT bundles are still present and visually not significantly altered, while the big impurity clusters lose their tubular constituents.

4 Residence time

By changing the diameter of the reactor tube from 85 mm (d_1) to 65 mm (d_2) the residence time τ of the catalyst particles in the reaction zone is changed with volume V of the reactor zone and flow rate q of the gas flow through the reactor tube according to

$$\frac{\tau_1}{\tau_2} = \frac{V_1 q_2}{V_2 q_1}$$

The flow rate composed of the methane input, the Helium carrier though thiophene and ferrocene, but mainly dominated by the hydrogen flow (0.8 l/min), was kept the same in both cases, therefore $q_1 = q_2 = q$.
For the 85 mm diameter tube, a 3-zone horizontal furnace was used, for the 65 mm tube a vertical furnace. However, the temperature profiles in the reactor tube were the same in both cases (Figure S2); the temperature profile being the same for both reactor tubes, we assume the same length l of the reaction zone.

$$\frac{\tau_1}{\tau_2} = \frac{A_1 l q}{A_2 l q} = \frac{(85/2)^2 \pi}{(65/2)^2 \pi} = 1.71$$

Therefore a reduction in diameter of 30% decreases the residence time of particles in the reaction zone by 71%.

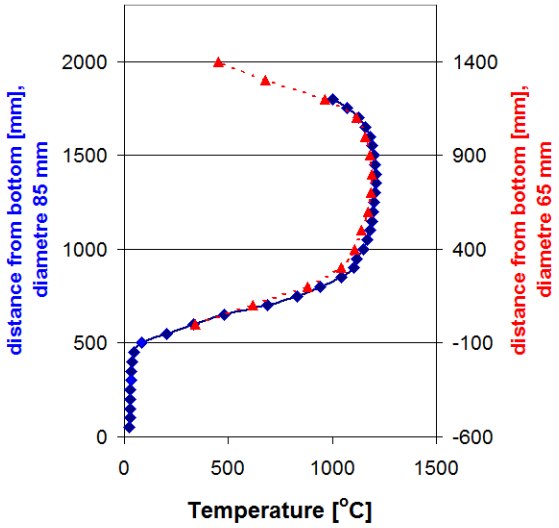

Figure S2: The temperature profile measured from the bottom for both the 85 mm (blue) and 65 mm (red) reactor tube.

5 Thermodynamic equilibria between iron, sulphur and hydrogen

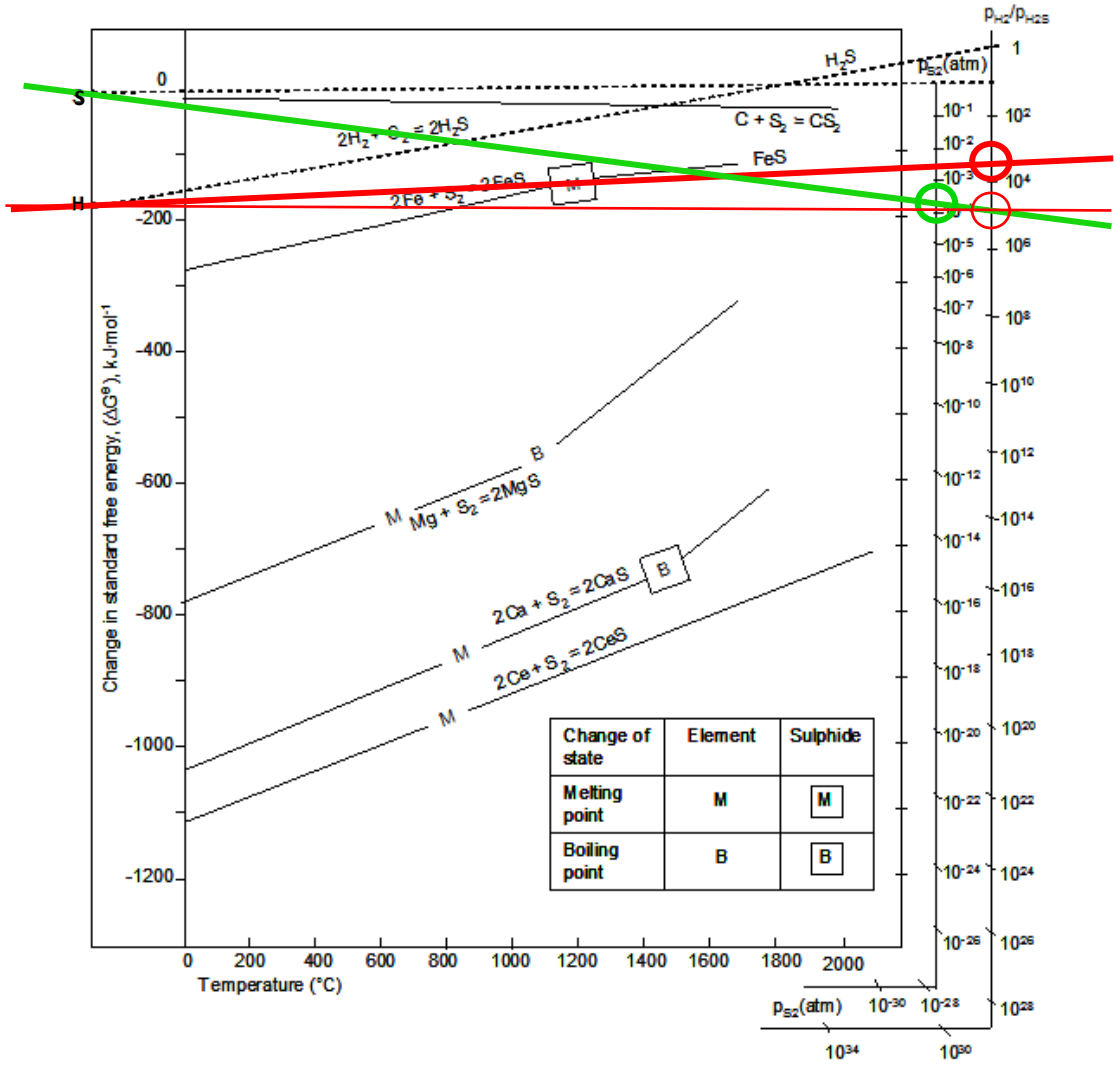

Figure S3: $\Delta G^{\ominus}$ – T diagram for sulphide formation. For calculation of equilibrium pS2 use points S and H respectively on the $\Delta G^{\ominus}$ axis. Re-drawn from [2]

These equilibria are expressed on the sulphide 'Ellingham diagram' shown in Figure S3. The actual equilibria depend on the partial pressures of sulphur in the gas phase (S_2) and the ratio of the partial pressures of hydrogen and hydrogen sulphide. A process factor is that the partial pressure of S_2 cannot exceed that supplied in the gas stream, which for standard conditions is 2❿10^{-4}, while the maximum ratio of H_2S/H_2 will similarly be limited to 4❿10^{-4} (on the diagram expressed as H_2/H_2S).

The green line superimposed on the diagram is the reference line for any equilibrium between a sulphide, the metal and S_2 gas at a partial pressure of 2❿ 10^{-4}, while the red line is for the reaction $2\ H_2 + S_2 = 2\ H_2S$ where the sulphur is in condensed form, and the ratio of partial pressures of H_2S/H_2 is 4❿ 10^{-4}. The first conclusion that can be drawn is, that for these given partial pressures, H_2S will be more stable than FeS at temperatures above 1150°C (Point where the red H_2S reaction line crosses the FeS one); whereas if the hydrogen was absent, the limiting partial pressure would only be reached above 1450°C (where the green reference line crosses the FeS one), and one would expect FeS to be stable up to this temperature under these conditions, which are not applicable here.

In making these predictions, we are aware that a coating of sulphur on the surface of the metal catalyst particles, even if covalently bonded to the metal is not the same phase as FeS. However, these equilibria give a basic starting point for understanding the likely stability of the sulphur coating on the catalyst particles, and the temperatures quoted are upper limits. They are firm however in indicating that any sulphur coating on the iron catalyst particles, will be lost to H_2S at the 'hot zone' set temperature of the reactor which is ~1300°C. The sulphide equilibrium lines for Ce, Ca and Mg are included in support of the discussion of sulphur in cast irons in SOM6. For the case of the low sulphur condition required to make single wall nanotube fibres, then the sulphur is predicted to be lost

from the catalyst at a temperature as low as 800°C. The dashed red line corresponds to the much lower maximum H_2S/H ratio possible under these conditions.

6 Sulphur in cast irons

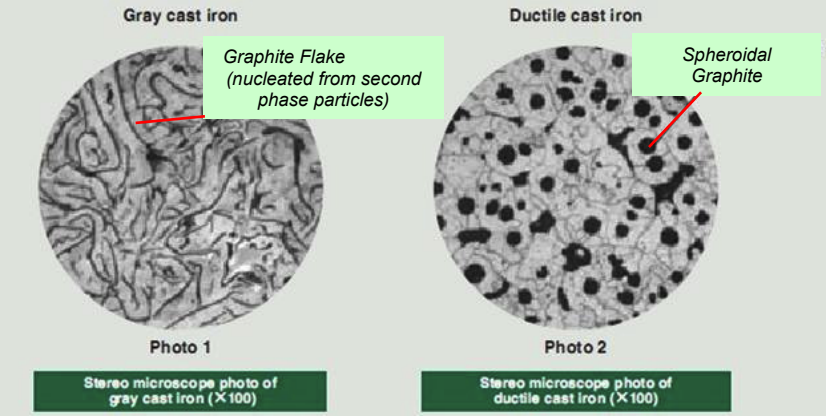

Figure S4: Metallographically prepared polished and etched sections showing microstructures of Grey cast iron (left) and Spheroidal Graphite cast iron (right).

The research field of cast irons, compared with that of carbon nanotubes, is highly mature. A comparatively new development (1947) has been the discovery by Millis [3] of a way of modifying the growth of graphite during the solidification process, so that instead of being present as flakes formed by edge growth, it is present in onion-like structures, which are much less effective at nucleating cracks. This tougher material is known as Speroidal Graphite (SG) cast iron or Ductile Cast Iron (Figure S4). It is produced by adding so-called inoculants to the molten metal, typically cerium, calcium and magnesium. It is probably the papers by Skaland, Grong and Grong [4,5] which throw most light onto the science behind this modification. These papers propose that it is the presence of sulphur which enhances edgewise growth, and that in general cast irons will have sufficient sulphur as a trace element, to favour this growth regime and form the graphite flakes typical for grey cast irons. Note from the Ellingham diagram (Figure S3) that cerium, calcium and magnesium form sulphides which are amongst the most stable of all sulphides, and thus are able to 'mop up' the sulphur dissolved in the liquid iron. Without sulphur, and noting that the absence of dissolved oxygen is also necessary, the graphite encapsulates its heterogeneous nucleating particle and by laying down successive layers gives net growth in the c-axis direction. The structure of such a spherulite in SG iron is depicted in Figure S5. The implication drawn from these references is that sulphur is an agent which greatly favours edgewise growth of graphitic material. In the field of cast iron science, sulphur is also widely recognised as a 'surfactant' in issues associated with the growth of graphitic structures in molten iron.

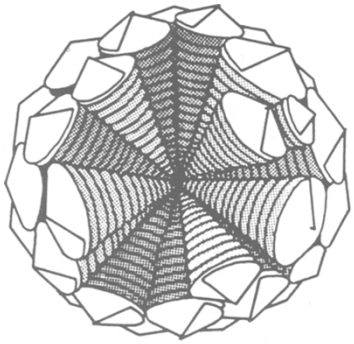

Figure S5: Sketch of the structure of a graphitic nodule in SG cast iron. The nodules grow in the direction of the graphite c axis.

7 Effect of winding speed / alignment of the bundles

For standard conditions, initially, increasing the winding speed (up to 30 m/min) leads to better alignment of the bundles and therefore better mechanical performance. However, the impurities, which do not contribute to the load bearing of the fibre, do not change in size. Therefore the voids formed by bundles bending around the impurities are stretched but not reduced in volume. For higher winding speeds > 30 m/min the linear density and the mechanical performance both decrease rapidly, as the number of bundles surrounding the voids decreases. I.e. rather than the positive effect of better alignment, we observe the worsening effect of the amount of voids dominating over the number of load bearing bundles.

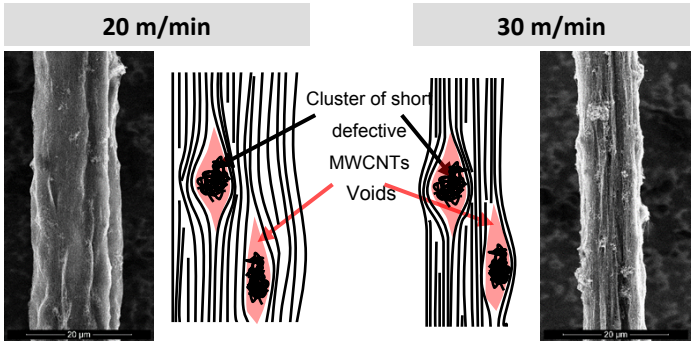

Figure S6: SEM images and schematics of the effect of different winding speed. A higher winding speed leads to better aligning of the load bearing bundles but not to a decrease of the impurity size.

In a tensile test, impurities mainly affect the initial part of stiffness, i.e. the initial slope of the stress-strain curve. The bent bundles stretch and align without taking up much load, before the contact quality and contact area between the bundles take over. In clean fibres, the structure is much better condensed and aligned, due to being void-free. Therefore we observe neither a flat-angle initial slope, nor the dominant effect of voids at higher winding speeds (Figure 12).

[1] G. Segre, and A. Silberberg, *Nature*, 1961, **189**, 209;

[2] J. J. Moore, 1981, *Chemical Metallurgy*, Butterworth & Co. (Publishers) Ltd

[3] K. Millis, *US patent 2485760*, "Cast Ferrous Alloy", issued 1949-10-25

[4] T. Skaland, O. Grong, and T. Grong, *Metal. Trans. A*, 1992, **23A**, 1333

[5] T. Skaland, O. Grong, and T. Grong, *Metal. Trans. A*, 1993, **24A,** 2347